

Identifiers

DOI 10.46298/jtcam.6906

OAI hal-03006177v3

History

Received Nov 16, 2020

Accepted Mar 10, 2021

Published May 27, 2021

Associate Editor

Anna Pandolfi

Reviewers

Maurizio Angelillo

Anna Pandolfi

Open Review

DOI 10.5281/zenodo.4813085

Supplementary Material

DOI 10.5281/zenodo.4034638

Licence

CC BY 4.0

©The Authors

Non steady-state intersonic cracks in elastomer membranes under large static strain

✉ Thomas CORRE^{1,2}, ✉ Michel CORET¹, ✉ Erwan VERRON¹, and Bruno LEBLÉ²¹ Institut de Recherche en Génie Civil et Mécanique, UMR CNRS 6183, École Centrale de Nantes, France² Naval Group Research, Technocampus Ocean, rue de l'Halbranne, 44340 Bouguenais, France

Dynamic crack propagation in elastomer membranes is investigated; the focus is laid on cracks reaching the speed of shear waves in the material. The specific experimental set-up developed to measure crack speed is presented in details. The protocol consists in (1) stretching an elastomer membrane under planar tension loading conditions, then (2) initiating a small crack on one side of the membrane. The crack speed is measured all along the crack path in both reference and current configurations, including both acceleration and deceleration phases, i.e. non steady-state crack propagation phases. The influence of the prescribed stretch ratio on crack speed is analysed in the light of both these new experiments and the few previously published studies. Conclusions previously drawn for steady-state crack growth are extended to non steady-state conditions: stretch perpendicular to the crack path governs crack speed in intersonic crack propagation regime, and the role of the stretch in crack direction is minor.

Keywords: dynamic fracture, elastomer, finite strain, non steady-state crack growth, intersonic regime.

1 Introduction

High speed fracture of elastomer membranes is a rather unusual problem for both fracture mechanics and elastomer engineering communities, mainly because of the narrow range of application and the complex context of both large strain and dynamics. Indeed, to our knowledge, only a dozen experimental studies on cracks combine large strain ($> 100\%$) and high speed propagation (close to the shear wave speed of the material) since the pioneering work of Treloar (1944). Peculiar features of such cracks have been highlighted, from wavy crack path (Stevenson and Thomas 1979; Deegan et al. 2001) to the role of strain-induced crystallisation in natural rubber (Zhang et al. 2009). The crack speed is naturally the mostly studied parameter of the problem. Thus, following the extension of the Griffith theory of fracture to elastomers by Rivlin and Thomas (1953), the relationship between crack speed and energy release rate is measured (Lake et al. 2000; Morishita et al. 2016). Alongside with this energetic approach, the precise role of strain in the membrane is investigated with both inflated (Stevenson and Thomas 1979; Moulinet and Adda-Bedia 2015) or plane (Gent and Marteny 1982a; Petersan et al. 2004) sheets of elastomer. In very recent works, the detailed strain field around the moving crack has been analysed with more recent full field measurement techniques (Corre et al. 2020; Mai et al. 2020). As a major result, it is established that crack speed increases with membrane deformation, ultimately reaching a limit which is assumed to be the velocity of the longitudinal waves in the material Moulinet and Adda-Bedia (2015). As common in fracture mechanics, the velocity of mechanical waves in the material is then used as a scaling factor. Because of the non-linear mechanical response of elastomers, such velocities are not easily computed: most of the authors propose empirical studies of wave propagation in parallel with their fracture experiments Gent and Marteny (1982b); Petersan et al. (2004). With direct measurements, Petersan et al. (2004) show that cracks can grow faster than shear waves in the stretched material, defining a crack propagation regime referred to as *intersonic*. Following the first observations of Gent and Marteny (1982a) and the theoretical derivation of Marder (2006), Chen et al. (2011) experimentally confirm

that crack speed in intersonic regime no longer scales with the energy release rate in the sample but with the stretch ratio; such results highly deviates from the standard linear fracture mechanics ones. In this regime, there is enough stored energy in the neighbourhood of the crack tip to maintain its propagation (Bouchbinder et al. 2010).

These studies on elastomer fracture attest the change in the mechanical quantity that drives crack growth at high speed but they exclusively concern steady-state propagation. From a more general point of view, the scrutiny of fast cracks with curved trajectories or changing speed is necessary to propose a predictive model for intersonic crack kinematics. It remains an experimental challenge for large strain problems. In this paper we propose a first step in this direction with a thorough analysis of the kinematics of a non-steady crack propagation. The classical pure shear sample is used but the propagation close to its edges, usually ignored, allows to observe accelerating and decelerating cracks with a straight crack path. Even in this rather simple context, careful assumptions have to be made to measure the instantaneous crack speed in both deformed and reference configurations. Several techniques coexist in the literature to estimate the shear wave speed, but they do not always clearly state the mechanical configuration to which it relates. In this study we propose the use of the little-known work of Boulanger and Hayes (1992) to clarify this computation. These kinematic assumptions and methods are detailed in Section 2 and put into practice with polyurethane samples in Section 3. In particular, results for intersonic cracks are discussed with respect to previous studies in Section 3.3 and Section 3.4 to shed some new light on this phenomenon.

2 Methods

2.1 Observing cracks: experimental set-up

For brevity, only the main features of the experimental set-up developed to monitor dynamic crack growth are presented; for more details the interested reader can refer to Corre et al. (2020) and extensive datasets are also available (DOI: [10.5281/zenodo.4034638](https://doi.org/10.5281/zenodo.4034638)).

“Pure shear” samples are considered: they are rectangular membranes with dimensions $200 \times 40 \times 3 \text{ mm}^3$. They are hold in a tensile machine along their longest sides (with molded bulges) in order to prescribe a vertical stretch ratio denoted λ_y . Practically, an experiment consists in the two steps presented in Figure 1(a):

- the sample is quasi-statically stretched (20 mm/min) until reaching the prescribed stretch ratio, it takes between 5 and 10 min;
- the crack is initiated by a small cut in one of the free edges of the sample, then it freely grows through the sample. The order of magnitude of propagation duration is 10 ms. The beginning of free crack propagation is defined by the moment when the crack tip moves faster than the blade ($\approx 0.6 \text{ m/s}$).

The first step is recorded with a high-resolution camera (29 Mpx) while the second step is recorded with a high-speed camera of which frame rate ranges between 7000 fps to 25 000 fps. Figure 1(b) shows an example of a picture taken during the crack growth step. The black speckle on the sample allows digital image correlation analysis during both steps. In particular, displacement and strain fields before crack propagation are measured, as illustrated in Figure 1(c). Pure shear samples are often used to observe steady-state crack propagation in the middle area of the sample where deformation is homogeneous (Gent and Marteny 1982b; Lake et al. 2000; Morishita et al. 2016). Here, we investigate the entire kinematics of the crack; this requires at least to know the strain state in the whole membrane.

2.2 Measuring crack speed

2.2.1 Definition of crack speed

In the seminal fracture theory of Griffith (1921), the propagation of a crack consists in dissipating energy by creation of new surfaces inside the material. These surfaces are usually considered in the reference configuration and the corresponding energetic driving quantities, classically the energy release rate, are defined with respect to the crack surface measured in this configuration Rivlin and Thomas (1953). Then, from this energetic point of view, the relevant crack speed is the rate at

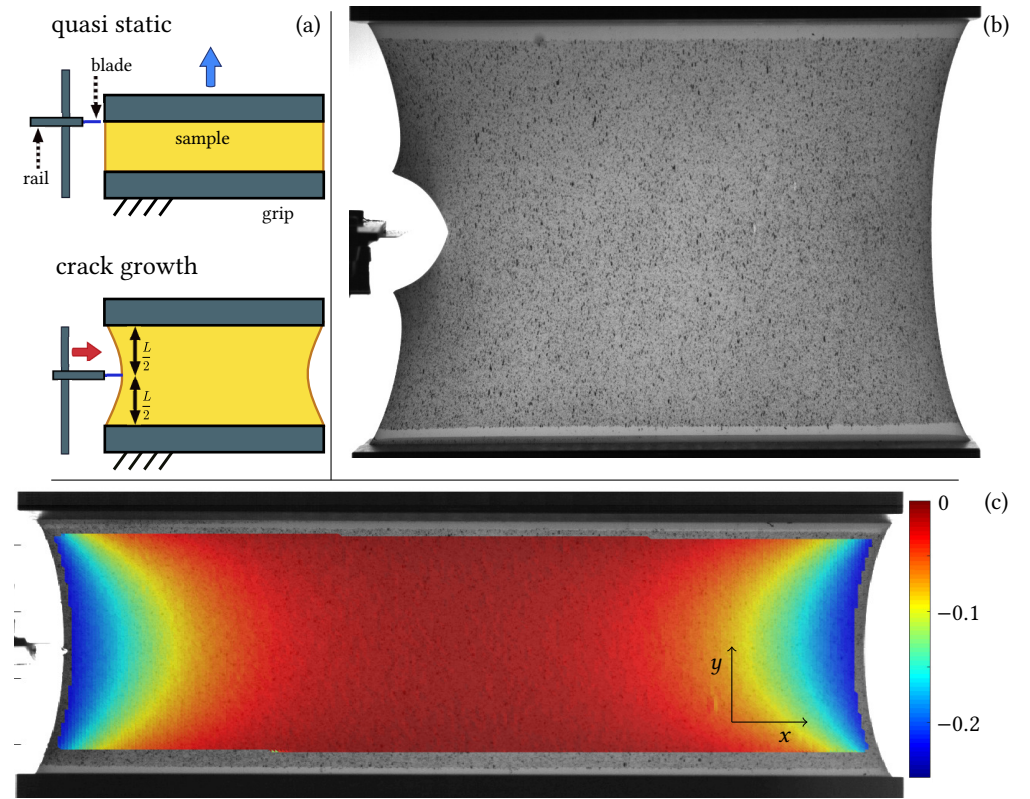


Figure 1 (a) The two step procedure. (b) Crack shape 0.6 ms after initiation (frame rate: 25 000 fps, shutter speed: 1/200 000 s). Prescribed stretch ratio $\lambda_y = 3.35$. (c) Strain field (component xx of the Green-Lagrange strain tensor) before crack growth. Prescribed stretch ratio $\lambda_y = 1.94$.

which these new surfaces are created. However, observing experimentally the rate of surface creation in largely deformed structures is not straightforward and we detail our method in the following.

The traditional approach to fracture considers geometric simplification to obtain a two-dimensional description of the problem. The crack front is then reduced to a point, located at the material point denoted $\vec{Z}(t)$ in the reference configuration that corresponds to the current time t , i.e. the undeformed sample which contains a crack, the length of which is defined at time t . The crack speed in the reference configuration can be defined as the speed of the crack tip $\vec{w}_0(t)$:

$$\vec{w}_0(t) = \frac{d\vec{Z}(t)}{dt}, \quad (1)$$

keeping a direct relationship with the rate of surface creation if the local width of the sample is known. Nevertheless, dynamic cracks are observed in deformed structures, thus the naked eye “sees” the crack speed in the deformed configuration. Let us denote $\vec{\chi}$ the mapping that transforms the position \vec{X} of a material point in the reference configuration to its position in the actual deformed configuration $\vec{x}(t) = \vec{\chi}(\vec{X}, t)$. At each time, the crack tip location in the deformed configuration is

$$\vec{z}(t) = \vec{\chi}(\vec{Z}, t), \quad (2)$$

and its time derivative is

$$\frac{d\vec{z}(t)}{dt} = \frac{\partial \vec{\chi}(\vec{Z}, t)}{\partial \vec{Z}} \frac{d\vec{Z}(t)}{dt} + \frac{\partial \vec{\chi}(\vec{Z}, t)}{\partial t}, \quad (3)$$

where

$$\mathbf{F}(\vec{Z}, t) = \frac{\partial \vec{\chi}(\vec{Z}, t)}{\partial \vec{Z}} \quad \text{and} \quad \vec{v}(\vec{Z}, t) = \frac{\partial \vec{\chi}(\vec{Z}, t)}{\partial t} \quad (4)$$

are the deformation gradient and the material velocity at crack tip, respectively. Thus, the relation between the crack speed in the deformed configuration \vec{w} and the crack speed in the reference configuration is

$$\vec{w} = \mathbf{F}\vec{w}_0 + \vec{v}. \quad (5)$$

For crack growth problems, the kinematic relationship (5) is applied to the successive locations of the crack tip, but it is to note that it is also valid for any sequence of location of a moving front in the material, such as a wave front as discussed in Section 2.3. In the most general case however, this formula is of little practical use to measure the crack speed as it requires precise measurements at crack tip to compute $\mathbf{F}(\vec{Z}, t)$ and $\vec{v}(\vec{Z}, t)$. Having chosen to monitor the whole sample, our set-up provide no measurements at less than about 2 mm from the crack tip (depending on the picture), as illustrated in Figure 2. Equation (5) is then bounded to be used

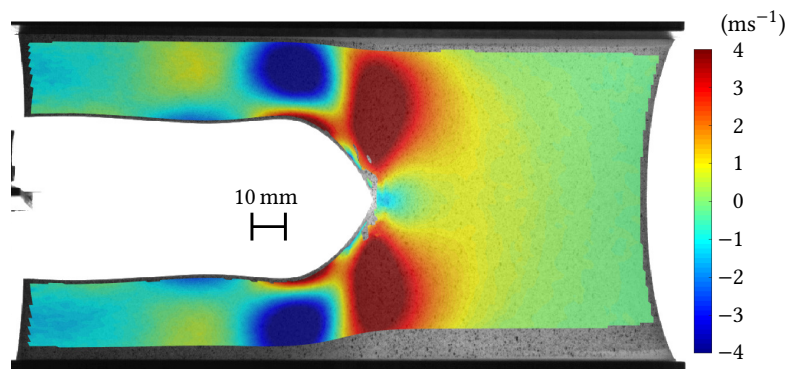


Figure 2 Horizontal velocity field during crack growth. The negative velocity in front of the tip indicates that the material is moving toward the crack tip. Some data are missing close to the tip because of the large shear strain and high velocities (image locally blurred) in this area. Prescribed stretch ratio: 2.41; crack speed: 45 m/s.

when these quantities are assumed *a priori*, that is to say when $\vec{v}(\vec{Z}, t) = 0$ (static membrane) and $\mathbf{F}(\vec{Z}, t)$ is constant (homogeneous strain field).

2.2.2 Practical computation of the crack speed

A possible way to overcome the above-mentioned lack of data consists in decomposing the displacement vector of the crack tip. For every material point \vec{X} of the sample, we denote \vec{x}_0 its position in the configuration at the end of the quasi-static loading step (without crack) and we recall that \vec{x} is its position in the cracked sample. Then the total displacement of \vec{X} is the sum of the displacement at the end of the quasi-static loading step, denoted \vec{u}_l , and the displacement during the second step, denoted \vec{u}_c . Adopting the Eulerian point of view,

$$\vec{u}_l(\vec{x}) = \vec{x}_0 - \vec{X} \quad \text{and} \quad \vec{u}_c(\vec{x}) = \vec{x} - \vec{x}_0. \quad (6)$$

Considering the particular case of the crack tip position $\vec{z}(t)$, it leads to

$$\vec{z}(t) = \vec{Z}(t) + \vec{u}_l(\vec{z}(t)) + \vec{u}_c(\vec{z}(t)). \quad (7)$$

During the second step, the propagation of the crack induces (measurable) movements of the material in its neighbourhood: in particular, the material situated in front of the crack tip moves toward it, as shown in Figure 2. More precisely, the horizontal component of $\vec{u}_c(\vec{z}(t))$ is negative and its vertical component is null when the crack grows along the middle line of the sample; its magnitude is unknown *a priori* but Goldman Boué et al. (2015) observe that it depends on the prescribed stretch ratio. In the following derivation, it is assumed that the displacement $\vec{u}_c(\vec{z}(t))$ is only due to the influence of the crack and does not include any large scale movement (oscillation, rigid body motion...). Moreover, if the crack does not cross a highly inhomogeneous displacement field (nor abrupt change in the thickness of the membrane), the effect of the displacement $\vec{u}_c(\vec{z}(t))$ on the successive crack tip positions $\vec{z}(t)$ can be neglected in Equation (7).

Thus, introducing \vec{z}_0 the position of the material point \vec{Z} at the end of the loading step, we have $\vec{z}(t) \approx \vec{z}_0(t)$ and the crack tip position in the reference configuration can be measured as

$$\vec{Z}(t) \approx \vec{z}(t) - \vec{u}_l(\vec{z}_0(t)). \quad (8)$$

Indeed, $\vec{z}(t)$ is directly observable on pictures, and $\vec{u}_l(\vec{z}_0(t))$ is obtained by projecting the successive locations of the crack tip $\vec{z}(t)$ onto the displacement field at crack initiation, which approximately corresponds to the first image of the high speed camera recording.

As a summary, the previous method consists in measuring the propagation of the crack tip neighbourhood, without considering the small movement of the crack tip in it. In the case of steady state propagation, the crack speed can be measured without this approximation: similar between two frames, \vec{u}_c has no influence. Note that it is no more the case for curved crack paths.

2.2.3 Application to our experiments

Equation (8) is now applied to our measurements. An example of such results is proposed in Figure 3(a), and Figure 3(b) compares the horizontal positions of the crack tip in both configurations during the experiment.

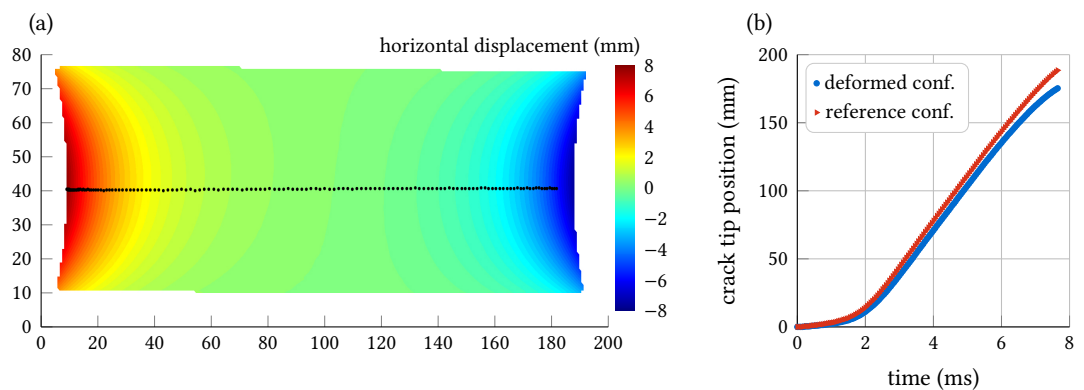


Figure 3 (a) Successive locations of the crack tip $\vec{z}(t)$ (black points) projected on the horizontal component of the displacement field $\vec{u}_l(\vec{z}_0(t))$ at the crack initiation moment. (b) Horizontal coordinate of the crack tip in both reference ($\vec{Z}(t)$) and deformed ($\vec{z}(t)$) configurations. The first observable position of the crack tip is set to 0. Prescribed stretch ratio: 1.94.

The time derivatives of $\vec{Z}(t)$ and $\vec{z}(t)$ provide the crack speed in both configurations. As the crack tip positions are measured at more or less one pixel (± 0.2 mm) and with a high temporal resolution, a standard finite difference scheme would lead to noisy results. Then these derivatives are computed with a local polynomial interpolation of order 2, over seven time steps. It is to note that the crack speed in the reference configuration cannot be computed at the end of the propagation: the right-hand side free edge largely moves when it enters in the neighbourhood of the crack, as shown in Figure 4. Then, the underlying hypotheses of Equation (8) no longer hold. Practically, pictures in which this phenomenon is noticeable (free edge moving toward the tip) are not taken into account during results analysis, as illustrated by the unfinished dotted line in Figure 3(a).

2.3 Shear wave speed in the material

The speed of mechanical waves plays a major role in dynamic fracture mechanics, as a limiting speed for cracks (Mott 1948) or as a scaling parameter (Dally 1979). The studies of cracks in elastomers illustrate this close connection between fracture and acoustics: Stevenson and Thomas (1979) propose an analytical study of wave propagation in their paper on bursting balloons, and Gent and Marteny (1982b); Gent and Marteny (1982a) study both fracture and waves in rubbers. More recently, Petersan et al. (2004) compare direct measurements of both cracks and plane waves speed in natural rubber sheets, and Marder (2006) theoretically explains these observations with the Mooney-Rivlin constitutive equation.

For linear elastic problems, well-established formulas provide analytical values for shear and longitudinal plane waves. However, for non-linear elastic problems, the speed of waves depends on

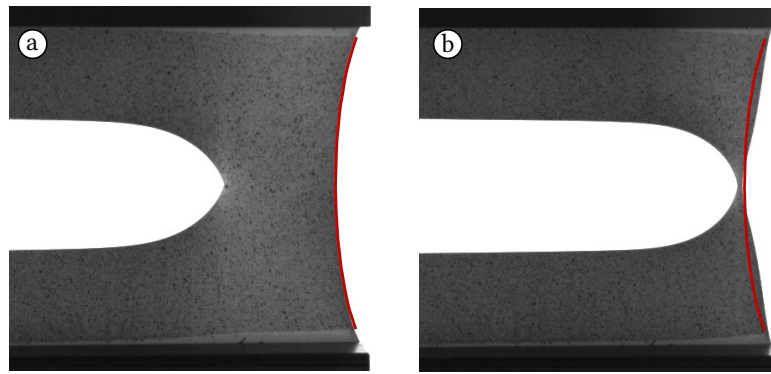


Figure 4 Deformation of the cracked sample; the red line represents the position of the free edge before crack initiation. (a) The shape of the free edge is not affected by the presence of the crack. (b) The shape of the free edge is highly modified. Prescribed stretch ratio: 1.94.

the mechanical response of the material, but also on the strain level and the propagation direction. Many of such wave propagation problems have been studied since the 1960s (Saccomandi 2007). Among them, we retain the work of Boulanger and Hayes (1992), who derive an analytical formula for the shear wave speed in a pre-stained Mooney-Rivlin material. In their study, authors consider the propagation of finite amplitude waves. This approach differs from many other studies that focus on small amplitude waves propagating in a homogeneously deformed medium. As this result is little known in the elastomer community, it is briefly recalled in the following.

Boulanger and Hayes (1992) consider an incompressible isotropic hyperelastic Mooney-Rivlin material; the corresponding strain energy density W per unit of undeformed volume is

$$W(I_1, I_2) = C_{10}(I_1 - 3) + C_{01}(I_2 - 3), \quad (9)$$

where C_{10} and C_{01} are the material parameters; $I_1 = \text{Tr}(\mathbf{B})$ and $I_2 = \frac{1}{2}(\text{Tr}(\mathbf{B})^2 - \text{Tr}(\mathbf{B}^2))$ are the first and second invariants of the left Cauchy-Green tensor $\mathbf{B} = \mathbf{F}\mathbf{F}^T$. The corresponding Cauchy stress tensor is $\boldsymbol{\sigma} = -p\mathbf{I} + 2C_{10}\mathbf{B} - 2C_{01}\mathbf{B}^{-1}$ where p is an (arbitrary) hydrostatic pressure due to the incompressibility assumption. As mentioned above, the authors derive the response of a pre-stretch membrane with superimposed finite amplitude waves; their results follows.

- For incompressible material, there are only shear waves (no longitudinal waves).
- For a shear wave that propagates in direction \vec{n} and is polarized in direction \vec{a} (i.e. inducing a displacement in the form $\vec{u} = f(\vec{n}, t)\vec{a}$ with respect to the pre-stretch state), a solution exists if

$$(\vec{n} \times \vec{a}) \cdot \mathbf{B}^{-1}\vec{a} = 0. \quad (10)$$

- Then, the corresponding shear wave speed in the deformed configuration is given by

$$\frac{1}{2}\rho c_s^2 = C_{10}\vec{n} \cdot \mathbf{B}\vec{n} + C_{01}\vec{a} \cdot \mathbf{B}^{-1}\vec{a}. \quad (11)$$

This equation relates the characteristics of the wave (\vec{n} , \vec{a} , and c_s), the material parameters (ρ , C_{10} and C_{01}), and the strain \mathbf{B} .

Finally, the corresponding wave speed in the reference configuration can be calculated with $\vec{C}_s = \mathbf{F}^{-1}c_s\vec{n}$ where \vec{C}_s is the shear wave vector in the reference configuration. Thus, the wave speed reads

$$\frac{1}{2}\rho C_s^2 = \vec{n} \cdot \mathbf{B}^{-1}\vec{n}(C_{10}\vec{n} \cdot \mathbf{B}\vec{n} + C_{01}\vec{a} \cdot \mathbf{B}^{-1}\vec{a}). \quad (12)$$

Note, that the density is the same in both configurations because the material is incompressible. This result provides an anisotropic wave speed in both reference and deformed configuration. This contradicts some expressions used in previous studies (Petersan et al. 2004; Mai et al. 2020).

2.4 Material model

The material is an unfilled polyurethane elastomer, its density ρ is 1044 kg/m^3 . Mooney-Rivlin parameters are determined with uniaxial tension experimental data: $C_{10} = 0.39 \text{ MPa}$ and $C_{01} = 0.97 \text{ MPa}$. The corresponding results are depicted in Figure 5. This hyperelastic model is used to compute the shear wave speed with the equations presented in Section 2.3.

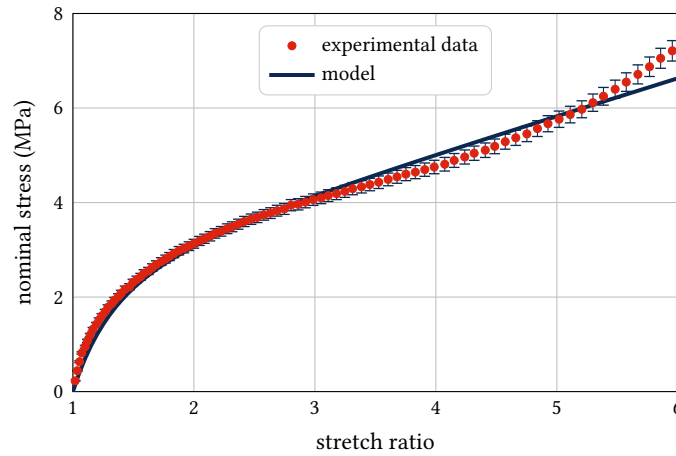


Figure 5 Quasi-static uniaxial tension of the material (strain rate: 0.001 s^{-1}).

3 Results and discussion

3.1 Preliminaries: shear wave speed for pure shear loading conditions

As stated above, the shear wave speed in the material depends on the strain state. In the middle of the sample, it corresponds to pure shear: denoting \vec{e}_x the horizontal direction (length of the sample), \vec{e}_y the vertical direction (height of the sample), and \vec{e}_z the out-of plane direction (thickness of the sample), the deformation gradient tensor is

$$\mathbf{F} = 1\vec{e}_x \otimes \vec{e}_x + \lambda_y \vec{e}_y \otimes \vec{e}_y + \frac{1}{\lambda_y} \vec{e}_z \otimes \vec{e}_z \quad (13)$$

where λ_y is the vertical stretch ratio prescribed during the experiment. Then, the left Cauchy-Green strain tensor is

$$\mathbf{B} = 1\vec{e}_x \otimes \vec{e}_x + \lambda_y^2 \vec{e}_y \otimes \vec{e}_y + \frac{1}{\lambda_y^2} \vec{e}_z \otimes \vec{e}_z. \quad (14)$$

The wave speed depends on the wave propagation \vec{n} and polarisation \vec{a} directions. In order to discuss the crack propagation speed with respect to the shear wave speed, it is relevant to consider the wave that propagates horizontally (like the crack) and is polarized vertically, i.e. $\vec{n} = \vec{e}_x$ and $\vec{a} = \vec{e}_y$. The corresponding shear wave speed in the deformed configuration given by Equation (11) is denoted by

$$c_{xy} = \sqrt{\frac{2}{\rho} \left(C_{10} + C_{01} \frac{1}{\lambda_y^2} \right)} \quad (15)$$

and Equation (12) states that its counterpart in the reference configuration C_{xy} simply reduces to

$$C_{xy} = c_{xy}, \quad (16)$$

i.e. the shear wave speeds in this direction are the same in both reference and deformed configurations. In other directions, it is no longer the case.

3.2 Steady-state crack growth

Experimental studies on dynamic fracture generally focus on steady state propagation: the crack speed measured in the homogeneously deformed part of the sample is plotted against the energy release rate (Lake et al. 2000; Morishita et al. 2016), against strain (Stevenson and Thomas 1979; Gent and Marteny 1982a; Petersan et al. 2004), or both (Zhang et al. 2009; Chen et al. 2011).

In the present case of pure shear samples, the crack propagates horizontally at constant speed in the middle of the sample; it corresponds to the linear part of curves in Figure 3(b). Note that these steady-state crack speeds in both reference and deformed configurations are equal: in the middle of the sample, the strain state is pure shear, i.e. $F_{xx} = 1$ and then $w\vec{e}_x = w_0\vec{e}_x$. Figure 6 gathers steady state crack speeds obtained for various samples and different prescribed stretch ratios λ_y ; the shear wave speed in corresponding uncracked samples are also plotted.

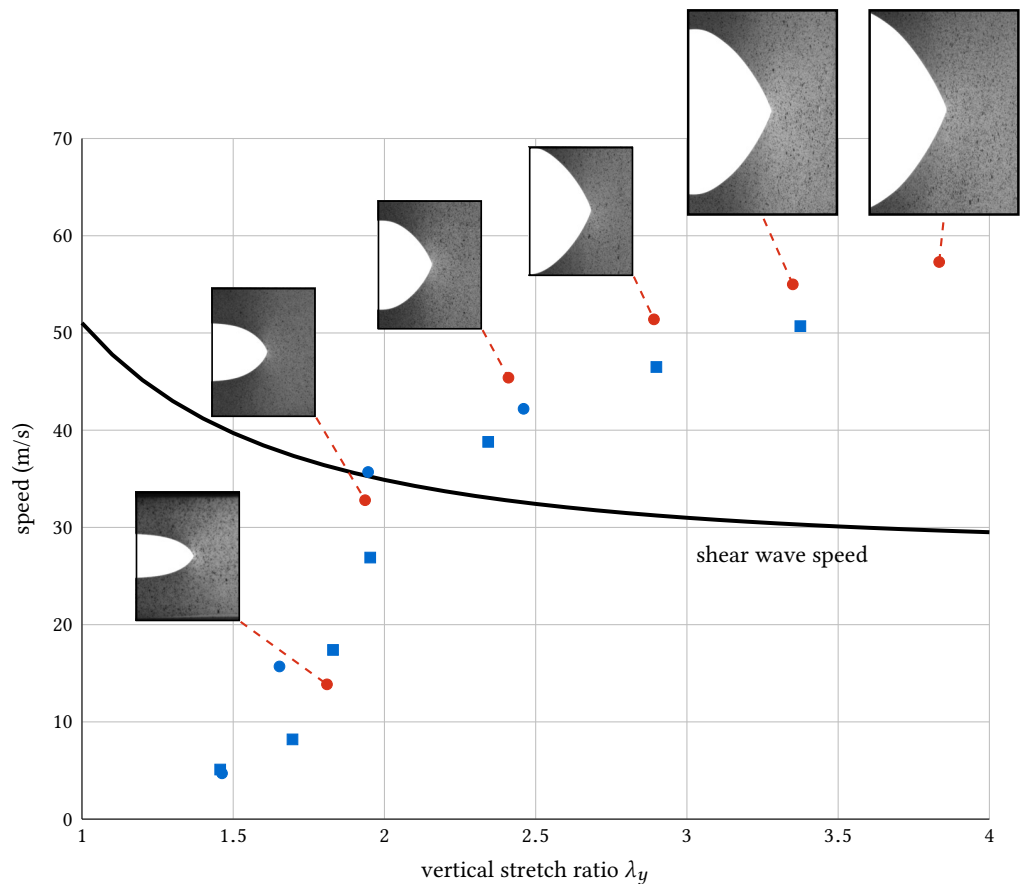


Figure 6 Shear wave and steady state crack propagation speeds vs. prescribed stretched ratio. Circles and squares refer to two different series of experiments (two batches of the same material). Pictures of crack tip and red dots indicate the experiments analysed in Section 3.3.

For small stretch ratios, the crack grows slower than the shear wave; the corresponding regime has been called “subsonic” (Marder 2006). For sufficiently large stretch ratios, here larger than two, the crack grows faster than the shear wave speed as previously observed by Petersan et al. (2004). This regime has been referred to as “inter-sonic” because the crack grows faster than the shear wave speed, but slower than the potential longitudinal wave speed (for compressible materials). A change in the slope of the crack speed curve is observed between these two regimes, albeit not as obvious as observed in natural rubber by Chen et al. (2011). Crack tip profiles also exhibit a progressive change from a parabolic to a wedge-like shape as previously reported by several authors (Zhang et al. 2009; Morishita et al. 2016).

3.3 Crack speed in the reference configuration

Figure 7 shows the instantaneous crack speed measured during crack growth in both reference and deformed configurations: for various prescribed stretch ratios, crack speed is plotted as a function of the distance traveled by the crack through the sample, namely the difference between

initial and current positions of the crack tip in the considered configuration. The curves that

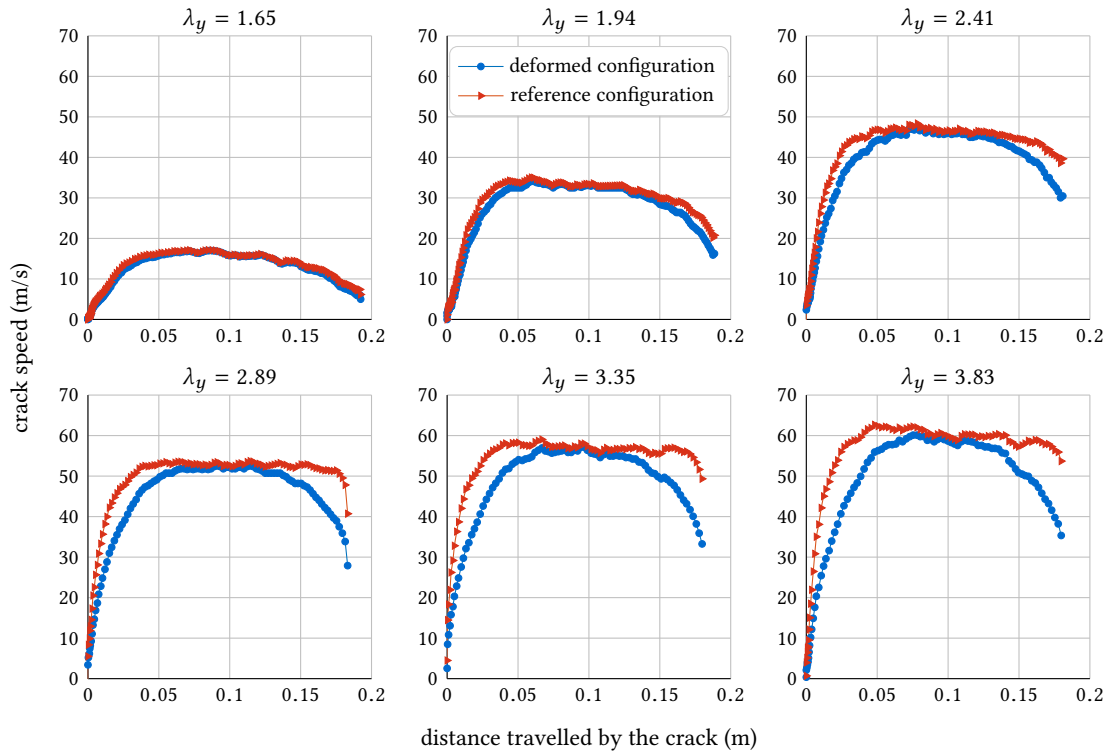


Figure 7 Instantaneous crack speed vs. distance traveled by the crack tip (in the reference configuration) for various prescribed stretch ratios.

correspond to the deformed configuration (blue circles in Figure 7) reflects what is directly visible on high speed camera films: the crack accelerates, then reaches a steady state propagation regime in the middle of the sample, and finally decelerates close to the free edge. Similar patterns are observed whatever the prescribed stretch ratio. However, observations in the reference configuration (red triangles in Figure 7) sometimes reveals a different behaviour: for some prescribed stretch ratios (the highest ones), the crack velocity remains constant close to the free edge, i.e. far from the homogeneously strained (pure shear) part of the sample. Note that even if the crack seems to decelerate at to the extremity of the sample, it must be considered with caution because of the difficulty to measure near the free edge (see Section 2.2.3). So, in the reference configuration, the evolution of crack speed during propagation depends on the prescribed stretch ratio. For low stretch ratios, the deceleration of the crack is the same in both configurations. The longest steady state crack growth plateau becomes clear for high stretch ratios, it can be considered as a loss of influence of the free edge on crack speed. If one refers to the previous Figure 6, the first two cases ($\lambda_y = 1.65$ and $\lambda_y = 1.94$) correspond to the subsonic propagation regime, while the other cases correspond to the intersonic propagation regime.

3.4 Discussion on the driving force of propagation regimes

In the previous sections, two novel (to the knowledge of the authors) results have been established: the use of the formula of Boulanger and Hayes for finite amplitude shear wave speeds, and the ability to measure the instantaneous speed of a crack in heterogeneous strain fields. Here, we intend to discuss these results with respect to previous works on dynamic fracture of elastomers, and to highlight some aspects of the problem which remain questionable.

Chen et al. (2011) argue that the change from a subsonic to an intersonic crack growth regime induces a change in the scaling regime. With pure shear samples and measuring steady-state crack growth, they observe that in the subsonic regime (low crack speeds) the energy release rate is the driving quantity (as expected from standard fracture mechanics), and that in the intersonic regime the crack speed scales with the prescribed stretch ratio. Their observations on steady-state crack growth can also explain our non-steady speed measurements. Indeed, the homogeneous

pure shear strain state in the sample corresponds to a constant energy release rate (Rivlin and Thomas 1953). However, when the crack reaches the neighbourhood of the right-hand side free edge, the strain state is more complex (no more homogeneous, it varies from pure shear to uniaxial tension) and the energy release rate changes with the crack tip position. Then, in the subsonic regime, the energy release rate changes when the crack tip approaches the free edge (see experiments with $\lambda_y = 1.65$ and $\lambda_y = 1.94$ in Figure 7). On the contrary, in the intersonic regime, the crack speed is governed by the local stretch ratio (perpendicular to the crack direction): as it is constant along the centreline of the sample, the crack speed is maintained to its steady-state value up to the close-edge area (see experiments with λ from 2.89 to 3.83 in Figure 7).

From a historical point of view, Gent and Marteny (1982a) were the first to observe that strain governs high speed crack growth. Our study allows us to revisit their seminal results. Gent and Marteny (1982a) investigated the growth of a crack in biaxially strained membranes. Their samples are similar to ours, and they measured the crack speed in the deformed configuration for various horizontal (direction of the crack) and vertical (normal to the crack direction) stretch levels. Two materials were studied: an unfilled and a carbon black-filled natural rubbers. In the following, only the results for the unfilled rubber are considered because, as stated by the authors, “relatively slow crack growth was observed for [the filled rubber]” and “the crack velocity was anomalously low”. Moreover, thanks to two other papers (Gent and Kim 1978; Gent and Marteny 1982b), it has been possible to roughly fit Mooney-Rivlin parameters for this unfilled rubber; considering their data, the model is valid up to stretch ratio of three. The corresponding values, i.e. $C_{10} = 0.08$ MPa and $C_{01} = 0.261$ MPa, the density of natural rubber, i.e. $\rho = 970$ kg/m³, and Equation (15) allows to determine the shear wave speed c_{xy} . The raw results of Gent and Marteny (1982a) are reproduced in Figure 8(a), with the shear wave speed. Three horizontal (crack direction) stretch are considered: $\lambda_x = 1$ corresponds to pure shear

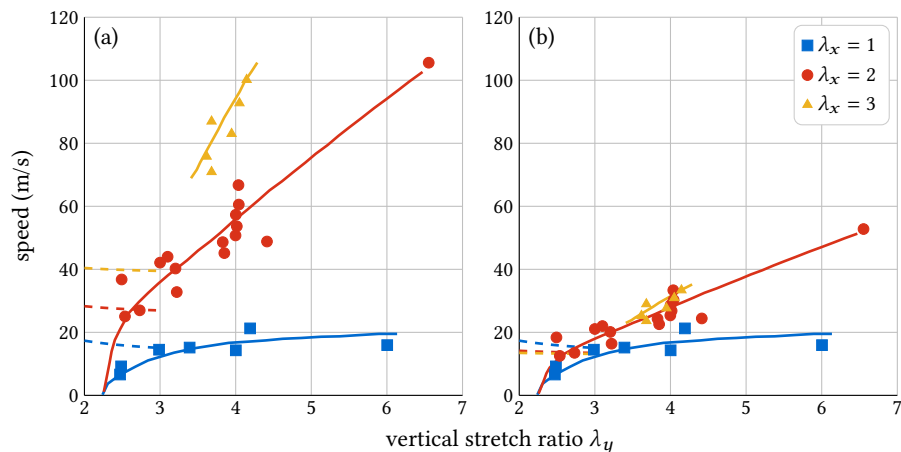


Figure 8 (a) Steady-state crack speed observed in unfilled natural rubber stretched membranes (λ_x, λ_y). Reproduction of Figure 4 from Gent and Marteny (1982a) (including the solid lines); dotted lines (not present in the original paper) indicate the corresponding shear wave speeds up to $\lambda_y = 3$. (b) Steady-state crack speed in the reference configuration.

and $\lambda_x = 2$ and 3 correspond to biaxial loading conditions. The crack speed in the reference configuration is calculated by Equation (5) assuming a static membrane and homogeneous strain field. The corresponding results are presented in Figure 8(b); note that the same scale has been adopted between results in deformed and reference configurations, and that the shear wave speeds are plotted according to Equation (16). Plotting data in the reference configuration reveals different features. Roughly speaking, the prescribed horizontal stretch ratio has very small effects, especially for $\lambda_x = 2$ and 3: the crack speed is governed by the vertical stretch λ_y and not by the energy release rate which differs with λ_x . Thus, for $\lambda_x \geq 2$, we argue that the cracks are in their intersonic regime. On the contrary, for $\lambda_x = 1$, the crack probably remains in its subsonic regime.

This interpretation is at least consistent with the results of Petersan et al. (2004) who highlight the weak effect of horizontal stretch ratio on crack speed, and with the present results. Indeed, we have shown that, in the reference configuration, crack speed is constant while the crack goes

through sample zones with different horizontal stretch ratio: it varies from $\lambda_x = 1$ in the middle of the sample to $\lambda_x = 1/\sqrt{\lambda_y}$ in the neighbourhood of the right-hand side free edge. In any case, it emphasizes the key role of the reference configuration in the understanding of crack growth: in our tests, the apparent deceleration of crack propagation observed in the deformed configuration corresponds in fact to a crack that propagates at constant speed in a compressed membrane ($\lambda_x < 1$).

4 Conclusion

The present study intends to continue the experimental exploration of rapid fracture in elastomer membranes; its novelty concerns the observation of non-steady crack propagation. The rarely mentioned assumptions required to measure properly the crack speed have been detailed. In particular, the set-up allows to compute the crack speed in both deformed and reference configurations. The method is completed with the exact formula of Boulanger and Hayes (1992) to calculate the shear wave speed in deformed samples: this analytical formula facilitates the kinematic analysis even if it necessitates the use of the Mooney-Rivlin model which is known to underestimate the large strain response of elastomers. The different behaviour observed for cracks between deformed and reference configurations, even in this pure shear sample, underlines the key role of the latter. This study advocates for the analysis of crack and wave propagation in the reference configuration, especially when even more complex underlying strain fields will be considered.

Our results confirm the previous observation of intersonic crack propagation, and notably at quite moderate strain level for industrial elastomers. They are also consistent with the particular scaling regime identified previously: at high speed, the crack speed is governed by the strain in the membrane and not by the energy release rate (as suggested by the standard theory). The present investigation and the new look taken to previous works (Gent and Marteny 1982a; Petersan et al. 2004) also underline the very small influence of the strain in the crack growth direction on the crack speed. Our observations provide a first experimental observation of the validity of these two results for a non steady-state propagation. The methods introduced here will be useful for the analysis of crack with varying crack speed and direction, in the pursuit of a model to predict fast crack kinematics in elastomers.

References

- Bouchbinder, E., J. Fineberg, and M. Marder (2010). Dynamics of simple cracks. *Annual Review of Condensed Matter Physics* 1(1):371–395. [DOI], [ARXIV].
- Boulanger, P. and M. Hayes (1992). Finite-amplitude waves in deformed Mooney-Rivlin materials. *The Quarterly Journal of Mechanics and Applied Mathematics* 45(4):575–593. [DOI].
- Chen, C. H., H. P. Zhang, J. Niemczura, K. Ravi-Chandar, and M. Marder (2011). Scaling of crack propagation in rubber sheets. *EPL (Europhysics Letters)* 96(3):36009. [DOI].
- Corre, T., M. Coret, E. Verron, B. Leblé, and F. Le Lay (2020). Experimental full field analysis for dynamic fracture of elastomer membranes. *International Journal of Fracture* 224(1):83–100. [DOI], [HAL].
- Dally, J. W. (1979). Dynamic photoelastic studies of fracture. *Experimental Mechanics* 19(10):349–361. [DOI].
- Deegan, R. D., P. J. Petersan, M. Marder, and H. L. Swinney (2001). Oscillating fracture paths in rubber. *Physical Review Letters* 88(1):014304. [DOI], [ARXIV].
- Gent, A. N. and H. J. Kim (1978). Tear strength of stretched rubber. *Rubber Chemistry and Technology* 51(1):35–44. [DOI].
- Gent, A. N. and P. Marteny (1982a). Crack velocities in natural rubber. *Journal of Materials Science* 17(10):2955–2960. [DOI].
- Gent, A. N. and P. Marteny (1982b). The effect of strain upon the velocity of sound and the velocity of free retraction for natural rubber. *Journal of Applied Physics* 53(9):6069–6075. [DOI].
- Goldman Boué, T., R. Harpaz, J. Fineberg, and E. Bouchbinder (2015). Failing softly: a fracture theory of highly-deformable materials. *Soft Matter* 11 (19):3812–3821. [DOI], [ARXIV].

- Griffith, A. A. (1921). The Phenomena of Rupture and Flow in Solids. *Philosophical Transactions of the Royal Society of London. Series A, Containing Papers of a Mathematical or Physical Character* 221(582-593):163–198. [DOI], [OA].
- Lake, G. J., C. C. Lawrence, and A. G. Thomas (2000). High-Speed Fracture of Elastomers: Part I. *Rubber Chemistry and Technology* 73(5):801–817. [DOI].
- Mai, T.-T., K. Okuno, K. Tsunoda, and K. Urayama (2020). Crack-Tip Strain Field in Supershear Crack of Elastomers. *ACS Macro Letters* 9(5):762–768. [DOI].
- Marder, M (2006). Supersonic rupture of rubber. *Journal of the Mechanics and Physics of Solids* 54(3):491–532. [DOI], [OA].
- Morishita, Y., K. Tsunoda, and K. Urayama (2016). Velocity transition in the crack growth dynamics of filled elastomers: Contributions of nonlinear viscoelasticity. *Physical Review E* 93(4):043001. [DOI].
- Mott, N. F. (1948). Brittle fracture in mild steel plates. *Engineering* 165:16–18.
- Moulinet, S. and M. Adda-Bedia (2015). Popping Balloons: A Case Study of Dynamical Fragmentation. *Physical Review Letters* 115(18):184301. [DOI].
- Petersan, P., R. Deegan, M. Marder, and H. Swinney (2004). Cracks in rubber under tension exceed the shear wave speed. *Physical Review Letters* 93(1):015504. [DOI], [ARXIV].
- Rivlin, R. S. and A. G. Thomas (1953). Rupture of rubber. I. Characteristic energy for tearing. *Journal of Polymer Science* 10(3):291–318. [DOI].
- Saccomandi, G. (2007). Finite Amplitude Waves in Nonlinear Elastodynamics and Related Theories: A Personal Overview? *Waves in Nonlinear Pre-Stressed Materials*. Springer Vienna, pp 129–179. [DOI].
- Stevenson, A and A. G. Thomas (1979). On the bursting of a balloon. *Journal of Physics D: Applied Physics* 12(12):2101–2109. [DOI].
- Treloar, L. R. G. (1944). Strains in an inflated rubber sheet, and the mechanism of bursting. *Rubber Chemistry and Technology* 17(4):957–967. [DOI].
- Zhang, H. P., J. Niemczura, G. Dennis, K. Ravi-Chandar, and M. Marder (2009). Toughening effect of strain-induced crystallites in natural rubber. *Physical Review Letters* 102(24):245503. [DOI].

Open Access This article is licensed under a Creative Commons Attribution 4.0 International License, which permits use, sharing, adaptation, distribution and reproduction in any medium or format, as long as you give appropriate credit to the original author(s) and the source, provide a link to the Creative Commons license, and indicate if changes were made. The images or other third party material in this article are included in the article's Creative Commons license, unless indicated otherwise in a credit line to the material. If material is not included in the article's Creative Commons license and your intended use is not permitted by statutory regulation or exceeds the permitted use, you will need to obtain permission directly from the authors—the copyright holder. To view a copy of this license, visit creativecommons.org/licenses/by/4.0. 

Authors' contributions Thomas Corre: conceptualization, investigation, writing original draft. Michel Coret: conceptualization, investigation, review and editing. Erwan Verron: conceptualization, review and editing. Bruno Leblé: resources, funding acquisition.

Supplementary Material Extensive datasets can be found at the permalink: [10.5281/zenodo.4034638](https://zenodo.org/record/4034638).

Ethics approval and consent to participate Not applicable.

Consent for publication Not applicable.

Competing interests The authors declare that they have no competing interests.

Journal's Note JTCAM remains neutral with regard to the content of the publication and institutional affiliations.